Journal of the Meteorological Society of Japan

EARLY ONLINE RELEASE

The DOI for this manuscript is
DOI:10.2151/jmsj.2025-038
J-STAGE Advance published date: November 4, 2025
The final manuscript after publication will replace the preliminary version at the above DOI once it is available.

Isotopic Signatures in Precipitation over the Southern and Central Tibetan Plateau Controlled by Active and Break Phases of the Indian Monsoon

Yutaka KUROSAKI[1], Akiyo YATAGAI[2],

1: Institute of Low Temperature Science
Hokkaido University, Sapporo, Japan
2: Graduate School of Science and Technology
Hirosaki University, Hirosaki, Japan

and

Atsuko SUGIMOTO[3]

3: Graduate School of Environmental Science
Hokkaido University, Sapporo, Japan

Revised Manuscript
Submitted to JMSJ (special issue)
Original submission: November 30, 2024
Revised submission: June 30, 2025
2nd revision: September 25, 2025

----

1) Corresponding author: Akiyo Yatagai, Graduate School of Science and Technology, Hirosaki University, 3 Bunkyocho, Hirosaki, Aomori 036-8152, JAPAN
Email: yatagai@hirosaki-u.ac.jp
Tel: +81-172-39-3685

Abstract

Stable isotopes in precipitation have been extensively evaluated across the Tibetan Plateau. However, the influence of distinct water vapor transport pathways on precipitation isotope ratios during the active and break phases of the Indian monsoon remains poorly understood. Temporal and spatial variations in these isotopes are documented over the Tibetan Plateau and Nepal based on the 1998 GEWEX-GAME/Tibet field campaign. According to these observations, the isotopic composition of precipitation over the plateau was strongly modulated by differences in water vapor transport mechanisms. The transport routes were classified into Indian monsoon and westerlies by employing backward trajectory analysis. The westerlies delivered precipitation with elevated $\delta^{18}O$ and d-excess values (d-excess = $\delta D - 8\delta^{18}O$) to the central Tibetan Plateau, consistent with the previous observations. In contrast, the Indian monsoon brought precipitation with distinct isotopic characteristics depending on the monsoon phase. During the active phase, the reduced rainfall south of the Himalayas limited the rainout of heavy isotopes, allowing water vapor with higher $\delta^{18}O$ than the break phase to reach the Tibetan Plateau. During the break phase, the enhanced orographic rainfall along the windward slopes of the Himalayas caused a progressive decrease in $\delta^{18}O$ values toward the north. These findings indicate that the accurate interpretation of stable isotope data in precipitation over the Tibetan Plateau requires consideration of both the active and break phases of the Indian monsoon.

Keywords: Stable isotopes in precipitation; Tibetan Plateau; Indian monsoon; Atmospheric moisture transport

1. Introduction

1.1 Climatic Significance of the Tibetan Plateau

The Tibetan Plateau serves as a critical heat source that influences monsoon circulation through direct and indirect mechanisms (e.g. Yanai et al., 1992; Kuwagata et al., 2001). This influence is exerted through surface-based heating of the middle atmosphere and latent heat released by convective clouds, which provide an additional thermal input. However, the middle atmosphere is usually very dry and the great Himalayan range acts as a barrier, preventing water vapor from entering the plateau. Consequently, the transport of water vapor to the Tibetan Plateau and adjacent semiarid regions has garnered extensive attention.

1.2 Intraseasonal Variability in the Indian Monsoon

The water cycle over the southern Tibetan Plateau is influenced by the Indian monsoon, a component of broader Asian monsoon system. Subseasonal fluctuations in rainfall, manifesting as alternating active and break phases, represent a key element of the variability of the Indian monsoon system (Ramamurthy, 1969). During the summer monsoon, the convection and precipitation patterns over central India exhibit marked intraseasonal variability, transitioning between active periods of substantial rainfall and break periods of minimal rainfall (Rajeevan et al., 2010; Singh et al., 2017). Notably, during these break phases over central India, precipitation often intensifies along the windward slopes of the Himalayas.

1.3 Stable Isotopes in Precipitation and Relevant Previous Studies

a. Basic Principles of Stable Isotopes and Deuterium (d)-excess in Precipitation

The stable isotopic composition of precipitation ($\delta^{18}O$ and δD) is influenced by hydrological processes, such as evaporation, mixing, transport, and precipitation history (Gat, 2010). In this context, deuterium excess (d-excess = $\delta D - 8\delta^{18}O$) reflects oceanic, lacustrine, and terrestrial surface conditions within moisture source regions and typically remains unchanged during condensation within transported air parcels (Merlivat and Jouzel, 1979). This unique property has been extensively applied in paleoclimate reconstruction using ice cores, particularly in the Tibetan Plateau (e.g., Thompson et al., 1989; Yao and Thompson, 1992; Thompson et al., 2000; Tian et al., 2003; Joswiak et al., 2013; Shao et al., 2017). Variations in temperature and atmospheric circulation are essential when interpreting ice core records, but variability in water vapor transport processes is equally critical. In particular, regional differences in water vapor transport characteristics and precipitation isotopic composition across the Tibetan Plateau must be considered (Yao et al., 2013, Man et al., 2022). Sun et al. (2019) demonstrated the influence of meteorological factors on stable isotope variations in the northwestern Tibetan Plateau, underscoring the role of transport pathways and atmospheric processes in shaping isotopic signatures across the region. Building on these insights, this study examines the southern and central Tibetan Plateau, excluding northern regions, and investigates precipitation isotopes and their associated transport processes in these areas.

b. Regional Classification of Precipitation Isotopes Across the Tibetan Plateau

Early studies on stable water isotopes in precipitation date back to field investigations conducted in the Himalayas between 1966 and 1968 (Zhang et al., 1973). Since the 1980s, monthly precipitation isotope data have been collected at Lhasa as part of the Global Network of Isotopes in Precipitation (GNIP), operated by the International Atomic Energy Agency (Yao et al., 2013). Subsequently, continuous monitoring of precipitation isotopes has been conducted at numerous sites across the Tibetan Plateau through the GNIP and the Tibetan Network for Isotopes in Precipitation (Yao et al., 2013, Man et al., 2022). Based on these observations, the spatial distribution of precipitation $\delta^{18}O$ across the Tibetan Plateau can be categorized into three domains according to differences in moisture sources and transport pathways: the monsoon domain in the southern plateau, the westerly domain in the northern plateau, and the transition domain in the central plateau (Yao et al., 2013). Li and Pang (2022) further supported this classification by identifying altitude-dependent isotope gradients in the eastern Tibetan Plateau.

In the monsoon domain, precipitation $\delta^{18}O$ values decrease during periods of strong southerly winds linked to the Indian monsoon, owing to progressive rainout along the moisture transport pathway (Tian et al., 2001b; Tian et al., 2003; Yao et al., 2013; Yu et al., 2015; Man et al., 2022). This interpretation was further corroborated by He and Richards

(2016), who demonstrated that $\delta^{18}O$ variability in precipitation across the Tibetan Plateau is chiefly governed by monsoon-driven moisture transport and rainout processes. In contrast, in the westerly domain of the northern Tibetan Plateau, precipitation is shaped by westerly winds and locally recycled water, with elevated $\delta^{18}O$ and d-excess values commonly observed during summer (Kurita and Yamada, 2008; Xu et al., 2011; Cui and Li, 2015; Sun et al., 2019). Meanwhile, within the transition domain, precipitation is influenced by both the Indian monsoon and the westerlies, and $\delta^{18}O$ values display stronger correlations with regional convective activity than with local meteorological conditions (Zhang et al., 2019).

1.4 Outstanding Challenges and the Significance of the 1998 Field Campaign

Previous studies have revealed that the spatial and temporal variations in $\delta^{18}O$ and d-excess levels in precipitation over the southern and central Tibetan Plateau cannot be fully explained by the simple rainout effect along the transport pathway (Tian et al., 2001; Gao et al., 2011; Yao et al., 2013; Man et al., 2022). He and Richards (2016) demonstrated that monsoon moisture exerted primary control on precipitation isotopes; however, the detailed distinction between the active and break phases of the Indian monsoon remains insufficiently understood.

The extreme elevation and limited accessibility of the Tibetan Plateau make field observations in this region particularly challenging. Under these circumstances, the comprehensive field campaign conducted in 1998 under the Global Energy and Water

Exchanges Project (GEWEX) and the GEWEX Asian Monsoon Experiment (GAME) yielded a uniquely valuable dataset. This campaign involved daily precipitation sampling, including d-excess, across multiple sites, as well as intensive sonde launches, ground-based meteorological measurements, and reanalysis dataset development. Furthermore, 1998 marked the beginning of observations by the Tropical Rainfall Measuring Mission/Precipitation Radar (TRMM/PR), the world's first satellite-borne radar capable of capturing the vertical structure of precipitation, including that over mountainous terrain. Ground-based Doppler radar measurements were also conducted in the same region. Together, these comprehensive datasets make 1998 a uniquely important year for advancing the understanding of precipitation processes over the southern and central Tibetan Plateau.

In recent years, numerical models incorporating water isotopes have reasonably reproduced $\delta^{18}O$ levels in precipitation; however, simulating d-excess, particularly under deep convective conditions, remains a major challenge. Moreover, the representation of isotope processes in non-hydrostatic models is still underway, and realistic simulations of d-excess have yet to be fully realized. Under these circumstances, accumulating reliable field-based observations is essential for interpreting stable water isotopes in paleoclimate studies, including ice core analyses.

1.5 Objectives of This Study

This study aims to clarify the relationship between the complex water vapor transport pathways and the stable isotopic composition ($\delta^{18}O$ and d-excess) of precipitation over the southern and central Tibetan Plateau. The study's findings are expected to provide valuable observational evidence supporting improvements in isotope-enabled models and past climate variability interpretation.

2. Materials

2.1 Observation and Sampling

The Tibetan Plateau features major east–west-extending mountain ranges exceeding 6,000 m in elevation, including the Himalayas, Nyainqentanglha Mountains, and Tanggula Mountains. In 1998, as part of the GEWEX-GAME, stable isotope monitoring of precipitation on the Tibetan Plateau was conducted during the Indian monsoon season. Precipitation samples were collected from April to September 1998 at Kathmandu (Nepal), Nyalam, Lhasa, Nagqu, AQB, and Amdo along a southwest–northeast transect across the Tibetan Plateau (Fig. 1). During the GEWEX-GAME/Tibet field campaign, daily precipitation samples Fig. 1 were collected each morning following rainfall events. Subsequently, the samples were analyzed for δD and $\delta^{18}O$ using a MAT 252 mass spectrometer equipped with a $CO_2/H_2/H_2O$ equilibration device at the Center for Ecological Research, Kyoto University. Here, analytical precision (1σ) was better than 0.2 ‰ for $\delta^{18}O$ and 2 ‰ for δD.

According to Yao et al. (2013), the Nyainqentanglha mountain range serves as a boundary, with the region to the south classified as the monsoon domain and the region to the north categorized as the transition domain. The temporal and spatial variability of precipitation isotopes was examined by distinguishing between the monsoon and transition domains.

2.2 Backward Trajectory

To identify the sources of water vapor associated with precipitation over the southern and central Tibetan Plateau, we applied the Hybrid Single-Particle Lagrangian Integrated Trajectory (HYSPLIT) model, developed by the National Oceanic and Atmospheric Administration (NOAA), using reanalysis data from the National Centers for Environmental Prediction (Stein et al., 2015). Doppler radar observations conducted in Nagqu in 1998 indicated that the echo-top height of 10 dBZ frequently exceeded 9.5 km above ground level (a.g.l.) on nearly all days between June 13 and September 19 (Uyeda et al., 2001). Based on the established characteristics of water vapor transport and the findings of Doppler radar observations, we conducted backward trajectory analyses from altitudes of 500, 1,500, 4,000, and 6,000 m a.g.l. at each observation site.

2.3 Meteorological Datasets

To examine precipitation during the study period across the monsoon Asia region, we used the Asian-Precipitation-Highly Resolved Observational Data Integration Toward Evaluation of Water Resources (APHRODITE) daily gridded precipitation dataset, derived from rain gauge observations (Yatagai et al., 2012). The target domain spanned 60°E–150°E and 15°N–55°N, with a spatial resolution of 0.5°. The analysis focused on the period from June to September 1998.

2.4 Satellite Datasets

To investigate the vertical distribution of precipitation, we relied on data from the PR onboard the TRMM (Iguchi et al., 1994). This satellite was a collaborative initiative between the National Aeronautics and Space Administration and the National Space Development Agency. The PR was developed by the Communications Research Laboratory among its five onboard instruments. It measured the radar backscatter from rainfall and the Earth's surface to characterize the three-dimensional structure of precipitation.

The PR was the world's first spaceborne precipitation radar and provided unprecedented vertical resolution of rainfall (Iguchi et al., 1994). In this study, we used rain rate data from the PR2A25 version 6 product. The horizontal and vertical resolutions were 4.3 and 0.25 km, respectively. The analysis focused on the period from June to September 1998.

3. Methods

3.1 Active and Break Phases of the Indian Monsoon

Periodic rainfall fluctuations over India are well documented. During the summer monsoon season of 1998, active and break phases of convective cloud development over India were observed through large-scale monitoring conducted by GAME as part of its intensive observation campaign from April to September (Matsumoto et al., 1999). According to these observations, the Indian monsoon period that year extended from June 10 to September 16. The first active phase began on June 10 over central India. This phase was followed by the first break phase, which began on July 10 and was accompanied by the development of an eastward-moving convective cloud system originating near 5°N, 65°E. The second active phase started on July 25, coinciding with northward-migrating convection over the Bay of Bengal. Subsequently, the second break phase began on August 15. Meanwhile, convective clouds over the equatorial Indian Ocean gradually moved northeastward and reached the Indian subcontinent on August 24. These developments appear to mark the onset of the third active phase over central India, which began on August 25. Ultimately, the Indian monsoon retreated from central India on September 16. Accordingly, the active phases of the Indian monsoon were recorded from June 10 to July 9 (day of year [DOY]: 161–190), July 25 to August 14 (DOY: 206–226), and August 25 to September 16 (DOY: 237–259) and are designated as a1, a2, and a3, respectively. The break phases recorded from July 10 to July 24 (DOY: 191–205) and August 15 to August 24 (DOY: 227–236) are referred to as b1 and b2, respectively.

3.2 Classification of Water Vapor Transport Pathways

We classified the transport routes into Indian monsoon and westerly pathways using backward trajectory analysis to examine the relationship between stable water isotopes in precipitation and associated water vapor transport pathways. Seven-day backward trajectories were calculated at heights of 500, 1500, 4000, and 6000 m above ground level. The classification of the Indian monsoon and westerly pathways was based on the following criteria. The Indian monsoon pathway was defined as the route along which water vapor originating from the Bay of Bengal or Arabian Sea crossed the southern slopes of the Himalayas via the Indian subcontinent. The westerly pathway was defined as the route along which water vapor originating from the Eurasian continent approached the Tibetan Plateau from the west or north without passing over the Indian subcontinent.

4. Results

4.1 Temporal and Spatial Variations in $\delta^{18}O$ and d-excess Levels in Precipitation

Figure 2 presents the spatial and temporal variations in $\delta^{18}O$ and d-excess levels. Within the monsoon domain, $\delta^{18}O$ values in Kathmandu were higher than those observed in Nyalam and Lhasa, with Nyalam exhibiting intermediate values. In other words, $\delta^{18}O$ generally decreased from south to north across the monsoon domain during the observation period. Meanwhile, temporal variations in $\delta^{18}O$ were similar across all sites, except during the a2 and b2 periods (July 31–August 21). $\delta^{18}O$ values were elevated during the early part of the a1 period, gradually decreased toward the middle of the b1 period, increased sharply at the onset of a2, steadily decreased toward the end of b2, and then gradually increased Fig. 2

toward the end of a3. During the a2–b2 interval, $\delta^{18}O$ values in Kathmandu remained elevated. In Nyalam, $\delta^{18}O$ values initially decreased during the early to middle portion of a2 and subsequently stabilized around −15 ‰ through the end of b2. In Lhasa, $\delta^{18}O$ generally decreased from the early part of a2 to the end of b2. Across the monsoon domain, $\delta^{18}O$ exhibited a slight periodic cycle aligned with the active and break phases of the Indian monsoon. Meanwhile, most d-excess values exhibited minimal variation throughout the observation period, remaining close to 10 ‰ at all sites.

In the transition domain, $\delta^{18}O$ values at the three sites remained largely comparable throughout the observation period, except during the middle of the a2 phase (July 30–August 5). During this interval, $\delta^{18}O$ values at AQB and Amdo were higher than those at Nagqu, indicating a south-to-north increase in $\delta^{18}O$ within the domain. Elevated $\delta^{18}O$ values were observed during the early and middle portions of a1, followed by a marked decline toward the end of this period. A comparable decreasing trend was evident during the b1 and a2 period, with values progressively declining from the beginning to the latter part of each period. During the b2 period, $\delta^{18}O$ values were lower than those in other periods and gradually increased toward the end of a3. Meanwhile, temporal variations in d-excess remained consistent across all three sites. Within the transition domain, d-excess values increased during active phases and decreased during break phases. However, across the observation period, d-excess exhibited a gradual upward trend. Elevated $\delta^{18}O$ and d-excess values were recorded in the middle portions of a1 and a2, and in the latter part of a3.

4.2 Flow Patterns Associated with the Active and Break Phases of the Indian Monsoon

Fig. 3

We classified the air parcel transport pathways as either the Indian monsoon or westerly pathways using seven-day backward trajectories (Fig. 3). Most air parcels arriving below the precipitation top height in the monsoon domain were associated with the Indian monsoon. In contrast, in the transition domain, while many parcels reaching 500 and 1500 m a.g.l. were transported by the Indian monsoon, a considerable proportion of those near the precipitation top height were transported by the westerlies.

4.3 Relationship Between Stable Water Isotopes and Water Vapor Transport Pathways

a. Monsoon Domain

Fig. 4

Fig. 5

The relationship between stable water isotopes in precipitation and air parcel transport pathways is illustrated in Figures 4 and 5. The $\delta^{18}O$ values in the monsoon domain decreased progressively from Kathmandu to Lhasa (Fig. 2). Meanwhile, the d-excess values exhibited minimal variation throughout the observation period, suggesting that the moisture source for precipitation remained relatively consistent across the domain (Fig. 2). Most of the water vapor contributing to precipitation in this region was transported by the Indian monsoon from the south of the Himalayas (Figs. 3, 4, S1, and S2). Air parcels reaching 1,500 m a.g.l. in Kathmandu, Nyalam, and Lhasa originated from the Bay of Bengal and the Arabian Sea (Fig. S1). In Lhasa, a substantial proportion of parcels were transported specifically from the Bay of Bengal (Fig. S1). The trajectories of these parcels were characterized by high specific humidity over the Indian subcontinent, which diminished along the southern slope of the Himalayas (Figs. S1 and S2). Moreover, the parcels ascended rapidly along the southern side of the Himalayas (Figs. S3 and S4).

b. Transition Domain

In the transition domain, $\delta^{18}O$ values were comparatively high during the early and middle stages of the a1, b1, and a2 periods and during the latter part of the a3 period (Fig. 2). During these intervals, air parcels arriving at the observation sites predominantly followed transport pathways linked to either the westerlies or the Indian monsoon (Figs. 3 and 4). When air parcels approached from the west or north under westerly influence, precipitation amounts declined, while $\delta^{18}O$ and d-excess values increased (Figs. 4 and 5). These westerly-derived air parcels displayed low specific humidity along their backward trajectories (Figs. S5 and S6) and followed higher-altitude trajectories (Figs. S7 and S8). In contrast, $\delta^{18}O$ values were lower during the b2 period and the latter stages of a1 and b1 (Fig. 2), when air parcels were primarily transported by the Indian monsoon (Fig. 4). During these periods, d-excess values declined to levels comparable to those in the monsoon domain (Fig. 5). These air parcels, which originated over the Indian subcontinent, displayed a south-to-north decline in specific humidity along their trajectories (Figs. S5 and S6). However, under the Indian monsoon regime during the active phase, $\delta^{18}O$ values were elevated in the early and middle stages of a1 and a2 (Fig. 4).

5. Discussion

5.1 Controlling Factors of $\delta^{18}O$ Values in Precipitation Across the Monsoon Domain

In the monsoon domain, this study recorded a south-to-north decrease in $\delta^{18}O$ values, attributed to the rainout effect between the Himalayas and the southern Tibetan Plateau, which is consistent with previous findings (Tian et al., 2001b; Tian et al., 2003; Yao et al., 2013; Yu et al., 2015; Man et al., 2022). Notably, the $\delta^{18}O$ values in Kathmandu did not exhibit a significant correlation with local precipitation, whereas those in Nyalam and Lhasa were weakly negatively correlated with precipitation at their respective sites (Figs. 4 and 6). This indicates that $\delta^{18}O$ levels in precipitation over southern Tibetan Plateau and Kathmandu do not reliably reflect local precipitation amounts. However, $\delta^{18}O$ levels in the monsoon domain exhibited a strong negative correlation with the amount of precipitation recorded in the south of the Himalayas 1–3 days earlier (Fig. 7). This region serves as the primary transport pathway for air parcels that deliver precipitation to the monsoon domain. Accordingly, $\delta^{18}O$ variations in this domain are predominantly governed by the precipitation amount along the trajectory of these air parcels.

Fig. 6

Fig. 7

Water vapor is transported from the south of the Himalayas to the southern Tibetan Plateau through multiple valleys, driven by the Indian monsoon. As moist air ascends along these valleys, heavy isotopes are progressively removed via precipitation, leading to isotopic depletion in the remaining vapor. Consequently, this Indian monsoon transport causes heavier water molecules to precipitate earlier in southern locations, such as Kathmandu, whereas lighter isotopes are transported farther north, producing a systematic decline in $\delta^{18}O$ throughout the region.

5.2 Influence of the Indian Monsoon Phases on Precipitation $\delta^{18}O$ in the Transition Domain

In the transition domain, $\delta^{18}O$ exhibited a negative correlation with local precipitation amounts (Figs. 4 and 6), consistent with previous findings (Yu et al., 2015; He and Richards, 2016). Precipitation linked to the westerlies was generally limited in volume and accompanied by elevated $\delta^{18}O$ and d-excess values throughout the observation period. Previous studies have reported that westerly-derived moisture includes recycled vapor from continental sources, which contributes to elevated $\delta^{18}O$ and d-excess values (Tian et al., 2001a; Tian et al., 2003; Kurita and Yamada, 2008). Accordingly, high $\delta^{18}O$ and d-excess values are expected when westerly influences primarily govern precipitation in the transition domain.

In contrast, Indian monsoon precipitation was relatively scarce and exhibited higher $\delta^{18}O$ values during the early and middle stages of a1 and a2, whereas it was more abundant and characterized by lower $\delta^{18}O$ values during b1, b2, and the latter part of a1. Instances in which water vapor transported by the Indian monsoon exhibits elevated $\delta^{18}O$ values are uncommon in the transition domain. In this study, such elevated $\delta^{18}O$ values associated with

Indian monsoon precipitation were mainly observed during the active phase of the Indian monsoon (a1 and a2). In the transition domain, $\delta^{18}O$ variations in Indian monsoon precipitation throughout the observation period showed a strong negative correlation with precipitation amounts recorded south of the Himalayas 1–3 days before the rainfall in the domain (Fig. 8). This southern Himalayan region served as the main transport corridor for air parcels carrying moisture to the transition domain via the Indian monsoon (Figs. S5–S8). Thus, $\delta^{18}O$ variations in Indian monsoon precipitation over the transition domain were predominantly controlled by upstream precipitation south of the Himalayas, consistent with the patterns observed in the monsoon domain. During the active phase of the Indian monsoon, the precipitation amounts showed a negative anomaly relative to the mean during the observation period (Fig. 9). Consequently, elevated $\delta^{18}O$ values in Indian monsoon precipitation during the active phase of the Indian monsoon were likely due to limited precipitation and reduced loss of heavy isotopes over the south of the Himalayas.

Fig. 8

Fig. 9

Although previous studies have attributed elevated $\delta^{18}O$ values in the transition domain to recycled moisture from land surfaces, Indian monsoon precipitation during the active phases of the Indian monsoon may have contributed to the observed increases in $\delta^{18}O$ values. We propose that stable water isotopes in precipitation over the southern and central Tibetan Plateau are potentially influenced by temporal variations in precipitation amounts associated with the active and break phases of the Indian monsoon in the south of the Himalayas.

6. Conclusion

Temporal and spatial variations in stable isotopes in precipitation were documented over the Tibetan Plateau and Nepal during the 1998 GEWEX-GAME/Tibet field campaign. These data revealed a relationship between stable precipitation isotopes and the Indian monsoon's meteorological patterns over the Tibetan Plateau.

In the monsoon domain, located in the southern part of the Tibetan Plateau and Nepal, $\delta^{18}O$ values decreased from Kathmandu to Lhasa. In contrast, the d-excess values showed little variation during the observation period. Most of the water vapor transported into the monsoon domain originated from south of the Himalayas and was associated with the Indian monsoon. Based on these findings, we suggest that the $\delta^{18}O$ composition of precipitation in the monsoon domain is primarily governed by monsoonal rainfall on the southern Himalayan slope.

In the transition domain of the central Tibetan Plateau, $\delta^{18}O$ values exhibited a strong negative correlation with local precipitation. When precipitation was influenced by water vapor transported by the westerlies, $\delta^{18}O$ and d-excess values were elevated. Westerly-transported air masses may have contained moisture recycled from continental sources, resulting in low precipitation amounts but relatively high $\delta^{18}O$ and d-excess values. When the Indian monsoon acted as the moisture source, $\delta^{18}O$ values were generally higher during its active phase and lower during the break phase. Precipitation in south of the Himalayas was reduced during the active phase compared with the break phase. This variation limited the rainout of heavier isotopes from water vapor, potentially increasing $\delta^{18}O$ values.

These findings highlight the importance of considering the active and break phases of the Indian monsoon when interpreting precipitation isotopic variations over the southern and central Tibetan Plateau.

Data Availability Statement

The water stable isotope dataset in this study is available from the corresponding author on request. The data of APHRODITE are available at http://aphrodite.st.hirosaki-u.ac.jp/products.html website. The ERA5 data was provided by ECMWF (https://www.ecmwf.int/en/forecasts/dataset/ecmwf-reanalysis-v5). The trajectories were calculated by the HYSPLIT model provided by NOAA (https://www.ready.noaa.gov/HYSPLIT.php). The TRMM PR data was provided by Japan Aerospace Exploration Agency (JAXA) (https://www.eorc.jaxa.jp/TRMM/index_e.htm). The ETOPO1 1 Arc-Minute Global Relief Model is provided by NOAA National Geophysical Data Center (https://www.ncei.noaa.gov/access/metadata/landing-page/bin/iso?id=gov.noaa.ngdc.mgg.dem:316).

Supplement

Supplementary Figures S1–S8 present the results of backward trajectory analyses.

Acknowledgments

We thank the late Prof. A. Numaguti for his guidance in precipitation sampling over the Tibetan Plateau. We also thank Dr. K. Ichiyanagi and Prof. L. Tian for their cooperation in sampling. Part of this work was supported by the Grant-in-Aid for scientific research (24K00701) from Japan Society for the Promotion of Science (JSPS).

References

Cui, B.-L., and X.-Y. Li, 2015: Stable isotopes reveal sources of precipitation in the Qinghai Lake Basin of the northeastern Tibetan Plateau. *Sci. Total Environ.*, **527–528**, 26–37, https://doi.org/10.1016/j.scitotenv.2015.04.105.

Curio, J., F. Maussion, and D. Scherer, 2015: A 12-year high-resolution climatology of atmospheric water transport over the Tibetan Plateau. *Earth Syst. Dyn.*, **6**, 109–124, https://doi.org/10.5194/esd-6-109-2015.

Gao, J., V. Masson-Delmotte, T. Yao, L. Tian, C. Risi, and G. Hoffmann, 2011: Precipitation Water Stable Isotopes in the South Tibetan Plateau: Observations and Modeling*. *J. Clim.*, **24**, 3161–3178, https://doi.org/10.1175/2010JCLI3736.1.

Gat, J. R., 2010: *Isotope hydrology: A study of the water cycle (Vol. 6)*.

He, S., and K. Richards, 2016: Stable isotopes in monsoon precipitation and water vapour in Nagqu, Tibet, and their implications for monsoon moisture. J. Hydrol., 540, 615–622, https://doi.org/10.1016/j.jhydrol.2016.06.046.

Iguchi, T., and R. Meneghini, 1994: Intercomparison of Single-Frequency Methods for Retrieving a Vertical Rain Profile from Airborne or Spaceborne Radar Data. *J. Atmospheric Ocean. Technol.*, **11**, 1507–1516, https://doi.org/10.1175/1520-0426(1994)011<1507:IOSFMF>2.0.CO;2.

Joswiak, D. R., T. Yao, G. Wu, L. Tian, and B. Xu, 2013: Ice-core evidence of westerly and monsoon moisture contributions in the central Tibetan Plateau. *J. Glaciol.*, **59**, 56–66, https://doi.org/10.3189/2013JoG12J035.

Juan, G., Z. Li, F. Qi, Y. Ruifeng, N. Tingting, Z. Baijuan, X. Jian, G. Wende, N. Fusen, D. Weixuan, Y. Anle, and L. Pengfei, 2020: Environmental effect and spatiotemporal pattern of stable isotopes in precipitation on the transition zone between the Tibetan Plateau and arid region. *Sci. Total Environ.*, **749**, 141559, https://doi.org/10.1016/j.scitotenv.2020.141559.

Kurita, N., and H. Yamada, 2008: The Role of Local Moisture Recycling Evaluated Using Stable Isotope Data from over the Middle of the Tibetan Plateau during the Monsoon Season. *J. Hydrometeorol.*, **9**, 760–775, https://doi.org/10.1175/2007JHM945.1.

Kuwagata, T., A. Numaguti, and N. Endo, 2001: Diurnal Variation of Water Vapor over the Central Tibetan Plateau during Summer. *J. Meteorol. Soc. Jpn.*, **79**, 401–418, https://doi.org/10.2151/jmsj.79.401.

Li, J., and Z. Pang, 2022: The elevation gradient of stable isotopes in precipitation in the eastern margin of Tibetan Plateau. *Sci. China Earth Sci.*, **65**, 1972–1984, https://doi.org/10.1007/s11430-021-9942-0.

Man, W., T. Zhou, J. Jiang, M. Zuo, and J. Hu, 2022: Moisture Sources and Climatic Controls of Precipitation Stable Isotopes Over the Tibetan Plateau in Water-Tagging Simulations. *J. Geophys. Res. Atmospheres*, **127**, e2021JD036321, https://doi.org/10.1029/2021JD036321.

Matsumoto, J., S. Xueshun, and A. Numaguti, 1999: GAME large-scale monitering for the intensive observation period, April-September 1998. *Cent. Clim. Syst. Res. Univ. Tokyo*.

Merlivat, L., and J. Jouzel, 1979: Global climatic interpretation of the deuterium-oxygen 18 relationship for precipitation. *J. Geophys. Res. Oceans*, **84**, 5029–5033, https://doi.org/10.1029/JC084iC08p05029.

Rajeevan, M., S. Gadgil, and J. Bhate, 2010: Active and break spells of the Indian summer monsoon. *J. Earth Syst. Sci.*, **119**, 229–247, https://doi.org/10.1007/s12040-010-0019-4.

Ramamurthy, K., 1969: Some aspects of the break in the Indian southwest monsoon during July and August. Forecasting Manual. *India Meteorol. Dep.*, **Part IV**.

Shao, L., L. Tian, Z. Cai, J. Cui, D. Zhu, Y. Chen, and L. Palcsu, 2017: Driver of the interannual variations of isotope in ice core from the middle of Tibetan Plateau. *Atmospheric Res.*, **188**, 48–54, https://doi.org/10.1016/j.atmosres.2017.01.006.

Singh, C., L. Thomas, and K. K. Kumar, 2017: Impact of aerosols and cloud parameters on Indian summer monsoon rain at intraseasonal scale: a diagnostic study. *Theor. Appl. Climatol.*, **127**, 381–392, https://doi.org/10.1007/s00704-015-1640-6.

Stein, A. F., R. R. Draxler, G. D. Rolph, B. J. B. Stunder, M. D. Cohen, and F. Ngan, 2015: NOAA's HYSPLIT Atmospheric Transport and Dispersion Modeling System. *Bull. Am. Meteorol. Soc.*, **96**, 2059–2077, https://doi.org/10.1175/BAMS-D-14-00110.1.

Sun, C., Y. Chen, J. Li, W. Chen, and X. Li, 2019: Stable isotope variations in precipitation in the northwesternmost Tibetan Plateau related to various meteorological controlling factors. *Atmospheric Res.*, **227**, 66–78, https://doi.org/10.1016/j.atmosres.2019.04.026.

Thompson, L. G., E. Mosley-Thompson, M. E. Davis, J. F. Bolzan, J. Dai, L. Klein, T. Yao, X. Wu, Z. Xie, and N. Gundestrup, 1989: Holocene—Late Pleistocene Climatic Ice Core Records from Qinghai-Tibetan Plateau. *Science*, **246**, 474–477, https://doi.org/10.1126/science.246.4929.474.

Thompson, L., T. Yao, E. Mosley-Thompson, M. E. Davis, K. A. Henderson, and P.-N. Lin, 2000: A High-Resolution Millennial Record of the South Asian Monsoon from Himalayan Ice Cores. *Science*, **289**, 1916–1919, https://doi.org/10.1126/science.289.5486.1916.

Tian, L., V. Masson-Delmotte, M. Stievenard, T. Yao, and J. Jouzel, 2001a: Tibetan Plateau summer monsoon northward extent revealed by measurements of water stable isotopes. *J. Geophys. Res. Atmospheres*, **106**, 28081–28088, https://doi.org/10.1029/2001JD900186.

Tian, L., T. Yao, A. Numaguti, and W. Sun, 2001b: Stable Isotope Variations in Monsoon Precipitation on the Tibetan Plateau. *J. Meteorol. Soc. Jpn.*, **79**, 959–966, https://doi.org/10.2151/jmsj.79.959.

Tian, L., T. Yao, P. F. Schuster, J. W. C. White, K. Ichiyanagi, E. Pendall, J. Pu, and W. Yu, 2003: Oxygen-18 concentrations in recent precipitation and ice cores on the Tibetan Plateau. *J. Geophys. Res. Atmospheres*, **108**, 2002JD002173, https://doi.org/10.1029/2002JD002173.

Tian, L., W. Yu, P. F. Schuster, R. Wen, Z. Cai, D. Wang, L. Shao, J. Cui, and X. Guo, 2020:

Control of seasonal water vapor isotope variations at Lhasa, southern Tibetan Plateau. *J. Hydrol.*, **580**, 124237, https://doi.org/10.1016/j.jhydrol.2019.124237.

Uyeda, H., H. Yamada, J. Horikomi, R. Shirooka, S. Shimizu, L. Liping, K. Ueno, H. Fujii, and T. Koike, 2001: Characteristics of Convective Clouds Observed by a Doppler Radar at Naqu on Tibetan Plateau during the GAME-Tibet IOP. *J. Meteorol. Soc. Jpn.*, **79**, 463–474, https://doi.org/10.2151/jmsj.79.463.

Wang, Z., A. Duan, S. Yang, and K. Ullah, 2017: Atmospheric moisture budget and its regulation on the variability of summer precipitation over the Tibetan Plateau. *J. Geophys. Res. Atmospheres*, **122**, 614–630, https://doi.org/10.1002/2016JD025515.

Webster, C. R., and A. J. Heymsfield, 2003: Water Isotope Ratios D/H,^{18} O/^{16} O, 17O/^{16} O in and out of Clouds Map Dehydration Pathways. *Science*, **302**, 1742–1745, https://doi.org/10.1126/science.1089496.

Xu, Y., S. Kang, Y. Zhang, and Y. Zhang, 2011: A method for estimating the contribution of evaporative vapor from Nam Co to local atmospheric vapor based on stable isotopes of water bodies. *Chin. Sci. Bull.*, **56**, 1511–1517, https://doi.org/10.1007/s11434-011-4467-2.

Yanai, M., C. Li, and Z. Song, 1992: Seasonal Heating of the Tibetan Plateau and Its Effects on the Evolution of the Asian Summer Monsoon. *J. Meteorol. Soc. Jpn.*, **70**, 319–351, https://doi.org/10.2151/jmsj1965.70.1B_319.

Yao, T., and L. G. Thompson, 1992: Trends and features of climatic changes in the past

5000 years recorded by the Dunde ice core. *Ann. Glaciol.*, **16**, 21–24, https://doi.org/10.3189/1992AoG16-1-21-24.

Yao, T., V. Masson-Delmotte, J. Gao, W. Yu, X. Yang, C. Risi, C. Sturm, M. Werner, H. Zhao, Y. He, W. Ren, L. Tian, C. Shi, and S. Hou, 2013: A review of climatic controls on δ^{18} O in precipitation over the Tibetan Plateau: Observations and simulations. *Rev. Geophys.*, **51**, 525–548, https://doi.org/10.1002/rog.20023.

Yatagai, A., K. Kamiguchi, O. Arakawa, A. Hamada, N. Yasutomi, and A. Kitoh, 2012: APHRODITE: Constructing a Long-Term Daily Gridded Precipitation Dataset for Asia Based on a Dense Network of Rain Gauges. *Bull. Am. Meteorol. Soc.*, **93**, 1401–1415, https://doi.org/10.1175/BAMS-D-11-00122.1.

Yu, W., L. Tian, Y. Ma, B. Xu, and D. Qu, 2015: Simultaneous monitoring of stable oxygen isotope composition in water vapour and precipitation over the central Tibetan Plateau. *Atmospheric Chem. Phys.*, **15**, 10251–10262, https://doi.org/10.5194/acp-15-10251-2015.

Yu, W., R. Guo, L. G. Thompson, J. Zhang, S. Lewis, Z. Jing, J. He, Y. Ma, B. Xu, G. Wu, X. Zhou, W. Tang, Q. Wang, P. Ren, Z. Zhang, and D. Qu, 2024: Water isotope ratios reflect convection intensity rather than rain type proportions in the pantropics. *Sci. Adv.*, **10**, eado3258, https://doi.org/10.1126/sciadv.ado3258.

Zhang, S., W. Yu, and Q. Zhang, 1973: Distribution of isotopes in some natural waters in the region north of Mt. Jolmo Lungma. *Sci. Sin.*, **16**, 560–564.

Zhang, T., Y. Zhang, Y. Guo, N. Ma, D. Dai, H. Song, D. Qu, and H. Gao, 2019: Controls of stable isotopes in precipitation on the central Tibetan Plateau: A seasonal perspective. *Quat. Int.*, **513**, 66–79, https://doi.org/10.1016/j.quaint.2019.03.031.

List of Figures

Fig. 1. Observation sites and topography of the Tibetan Plateau. Observation sites are indicated by circles. Shaded colors represent elevation based on the ETOPO1 model.

Fig. 2. Spatial and temporal variations in δ18O and d-excess during the 1998 Indian monsoon. Orange and blue shaded areas indicate the active (a1, a2, a3) and break (b1, b2) phases, respectively.

Fig. 3. Temporal variations in precipitation top height (light green) and moisture transport pathways. Water vapor transport routes were classified as continental or Indian monsoon based on seven-day backward trajectories initiated at 6000 m a.g.l. (A), 4000 m a.g.l. (B), 1500 m a.g.l. (C), and 500 m a.g.l. (D). Labels a1–a3 represent the active phase, and labels b1–b2 represent the break phase.

Fig. 4. Temporal variations in $\delta^{18}O$ and precipitation at each observation site. $\delta^{18}O$ data points were classified by the transport pathways of air parcels, identified using backward trajectories and meteorological fields over the Tibetan Plateau and India. Indian monsoon and westerly flows were distinguished using seven-day backward trajectories. Grey shaded boxplots denote the daily precipitation amount. *r* and *p* values denote the Pearson correlation coefficient and its statistical significance between $\delta^{18}O$ and precipitation, respectively.

Fig. 5. Temporal variations in d-excess and precipitation at each observation site. d-excess data points were classified according to the transport pathways of air parcels, identified

using backward trajectories and meteorological fields over the Tibetan Plateau and India. Indian monsoon and westerly flows were distinguished using seven-day backward trajectories. Grey shaded boxplots denote the daily precipitation amount. *r* and *p* values denote the Pearson correlation coefficient and its statistical significance between d-excess and precipitation, respectively.

Fig. 6. Correlation coefficients between $\delta^{18}O$ in precipitation at each site and precipitation amount. Black contoured regions indicate p < 0.05 based on Student's t-test. Site positions are represented by a white circle (Kathmandu), triangle (Nyalam), hexagon (Lhasa), square (Nagqu), inverted triangle (AQB), and star (Amdo).

Fig. 7. Correlation coefficients between $\delta^{18}O$ values in precipitation at three sites: Kathmandu (left), Nyalam (center), and Lhasa (right), and precipitation amounts at time lags of one day (top), two days (middle), and three days (bottom). Black contoured regions indicate p < 0.05 based on Student's *t*-test. The positions of the sites are represented as follows: white circle (Kathmandu), triangle (Nyalam), and hexagon (Lhasa).

Fig. 8. Correlation coefficients between $\delta^{18}O$ values associated with Indian monsoon precipitation at three sites: Nagqu (left), AQB (center), and Amdo (right), and precipitation amounts at time lags of one day (top), two days (middle), and three days (bottom). Black contoured regions indicate p < 0.05 based on Student's *t*-test. Site positions are indicated by a white square (Nagqu), inverted triangle (AQB), and star (Amdo).

Fig. 9. Mean precipitation anomalies during the active (a1, a2, and a3) and break (b1 and

b2) phases of the Indian monsoon, based on the APHRODITE dataset. Daily precipitation anomalies were calculated as the difference between daily precipitation and the mean precipitation over the entire observation period. Site positions are indicated by a white circle (Kathmandu), triangle (Nyalam), hexagon (Lhasa), square (Nagqu), inverted triangle (AQB), and star (Amdo).

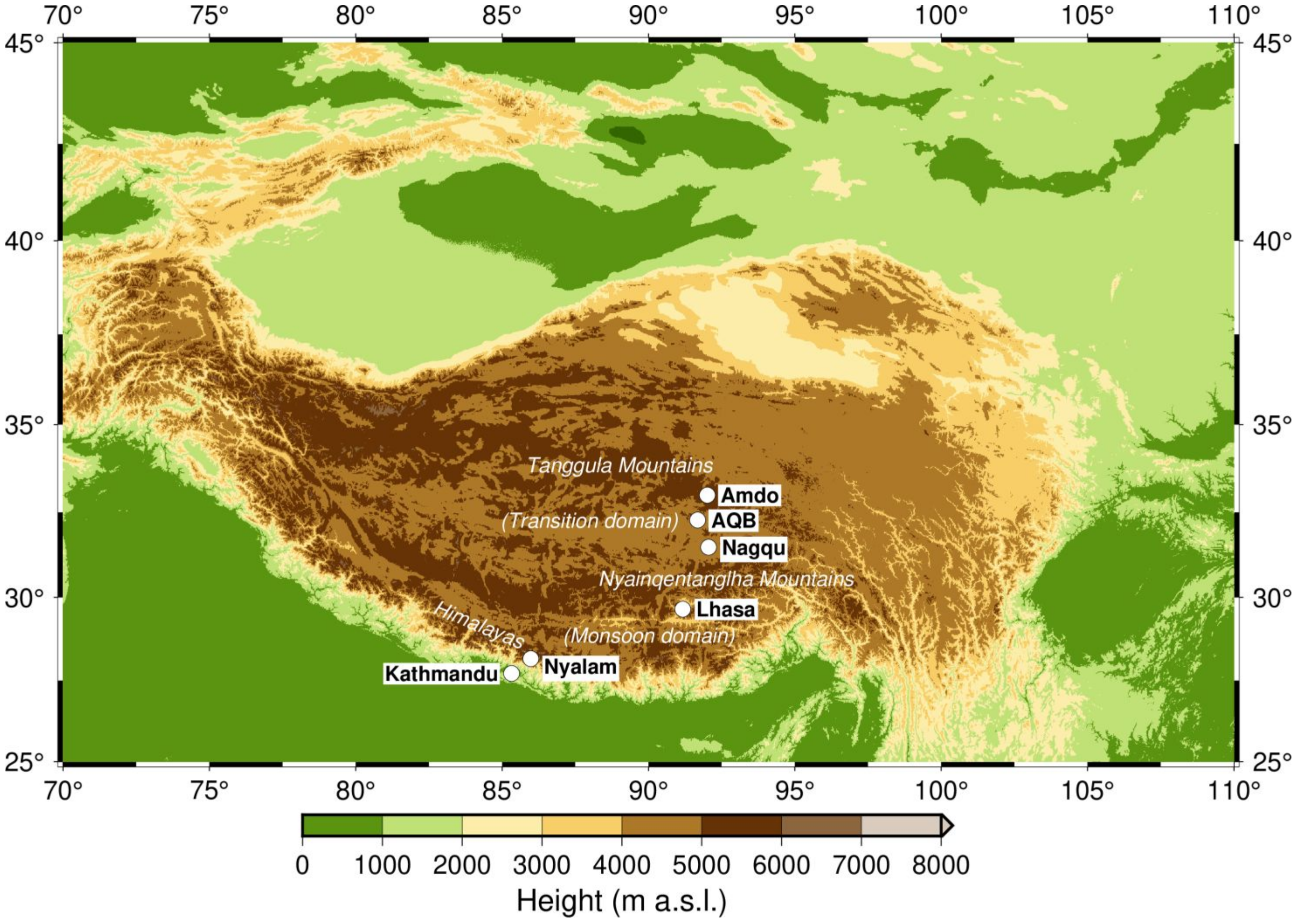

Fig. 1. Observation sites and topography of the Tibetan Plateau. Observation sites are indicated by circles. Shaded colors represent elevation based on the ETOPO1 model.

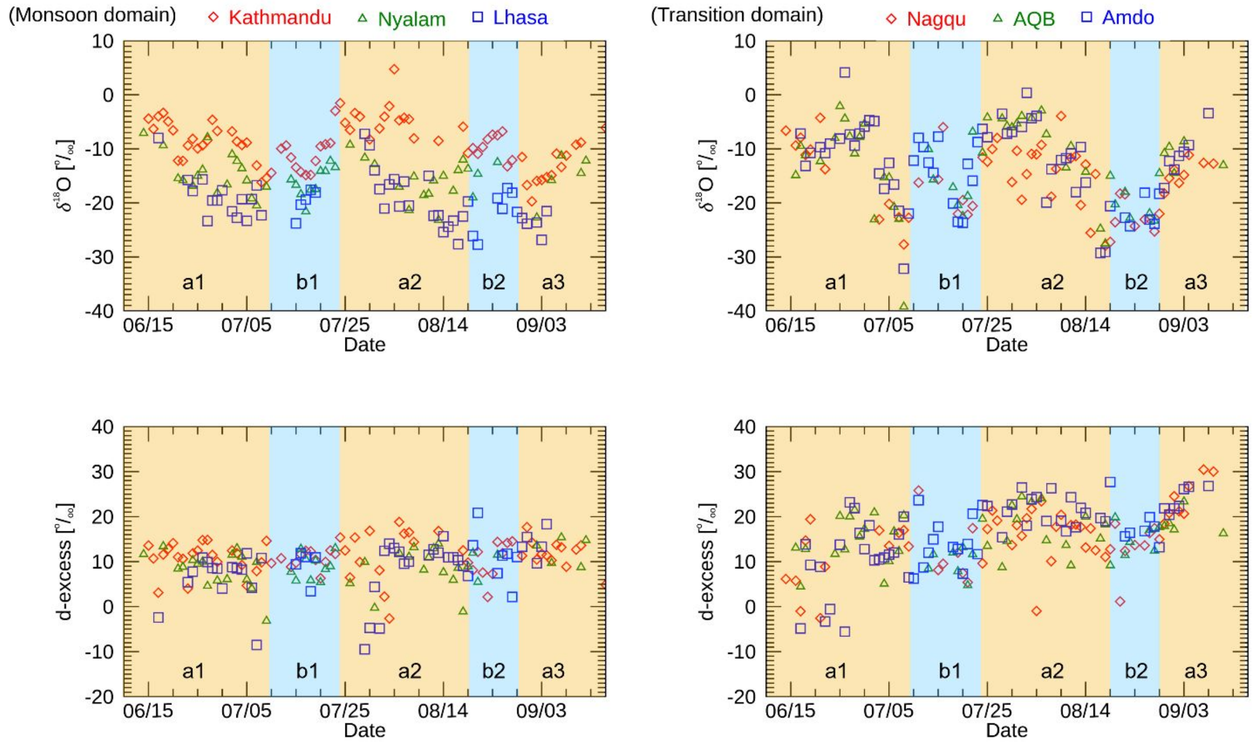

Fig. 2. Spatial and temporal variations in $\delta^{18}O$ and d-excess during the 1998 Indian monsoon. Orange and blue shaded areas indicate the active (a1, a2, a3) and break (b1, b2) phases, respectively.

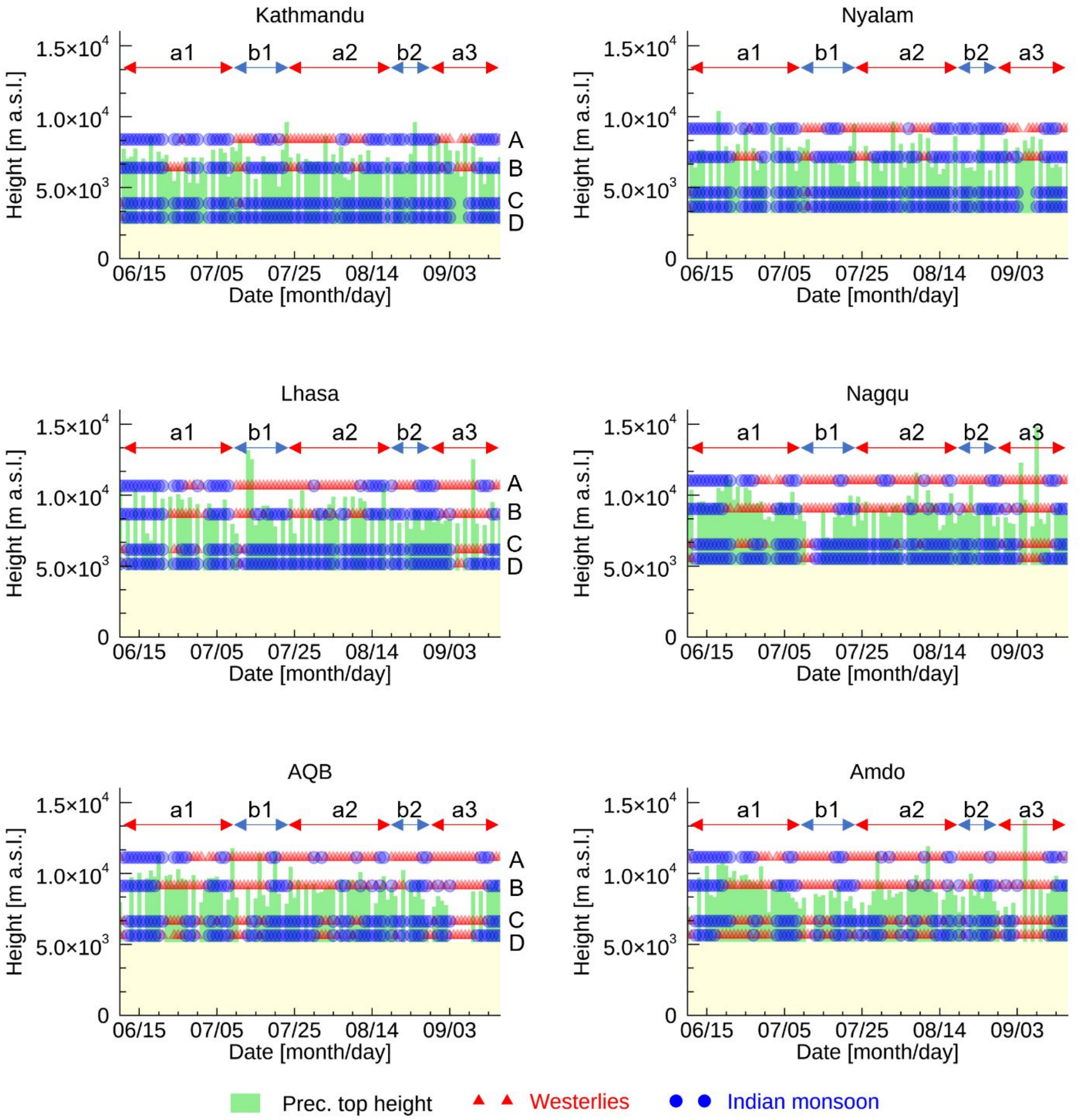

Fig. 3. Temporal variations in precipitation top height (light green) and moisture transport pathways. Water vapor transport routes were classified as westerlies or Indian monsoon based on seven-day backward trajectories initiated at 6000 m a.g.l. (A), 4000 m a.g.l. (B), 1500 m a.g.l. (C), and 500 m a.g.l. (D). Labels a1–a3 represent the active phase, and labels b1–b2 represent the break phase.

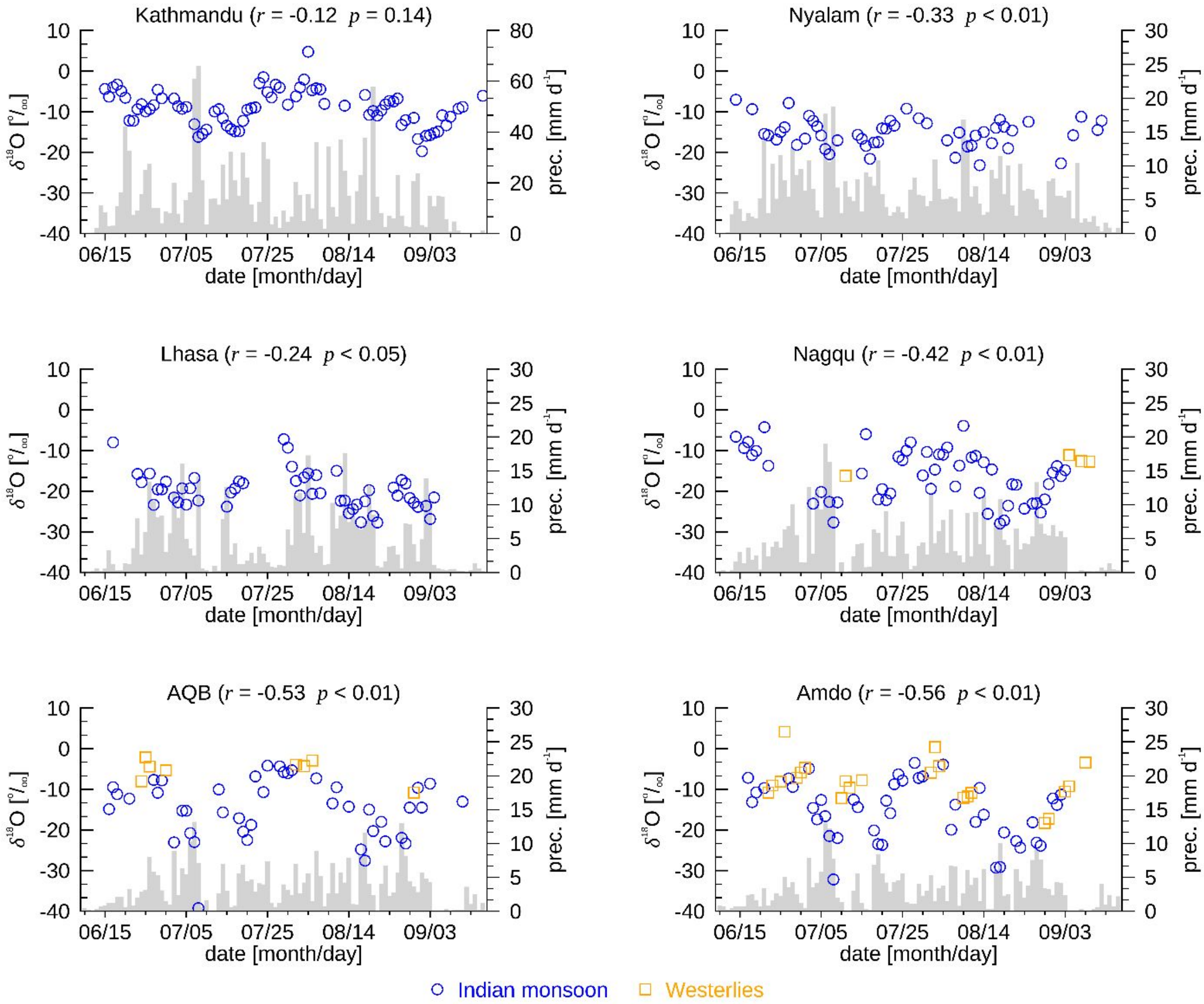

Fig. 4. Temporal variations in δ18O and precipitation at each observation site. δ18O data points were classified by the transport pathways of air parcels, identified using backward trajectories and meteorological fields over the Tibetan Plateau and India. Indian monsoon and westerly flows were distinguished using seven-day backward trajectories. Grey shaded boxplots denote the daily precipitation amount. *r* and *p* values denote the Pearson correlation coefficient and its statistical significance between δ18O and precipitation, respectively.

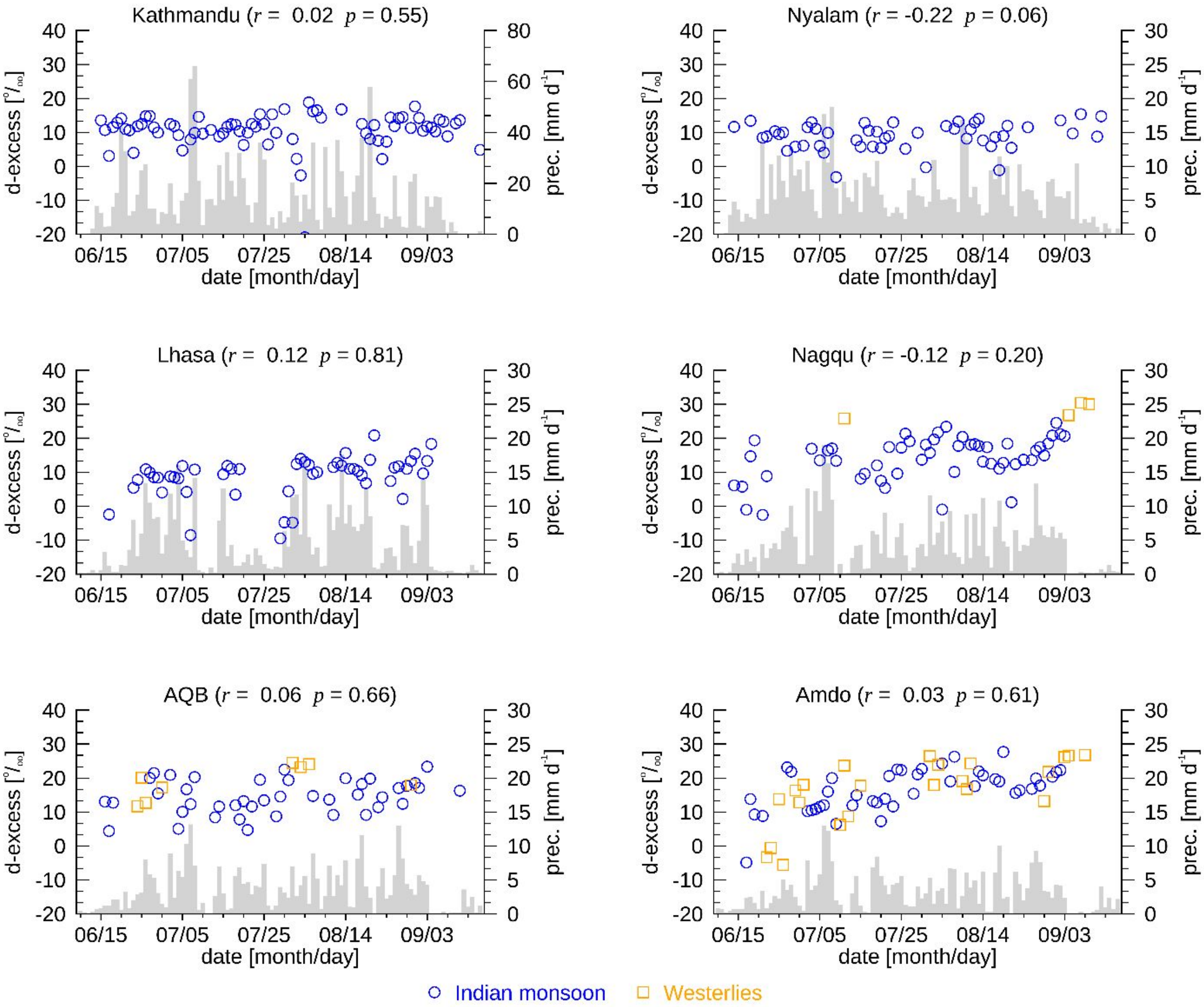

Fig. 5. Temporal variations in d-excess and precipitation at each observation site. d-excess data points were classified according to the transport pathways of air parcels, identified using backward trajectories and meteorological fields over the Tibetan Plateau and India. Indian monsoon and westerly flows were distinguished using seven-day backward trajectories. Grey shaded boxplots denote the daily precipitation amount. *r* and *p* values denote the Pearson correlation coefficient and its statistical significance between d-excess and precipitation, respectively.

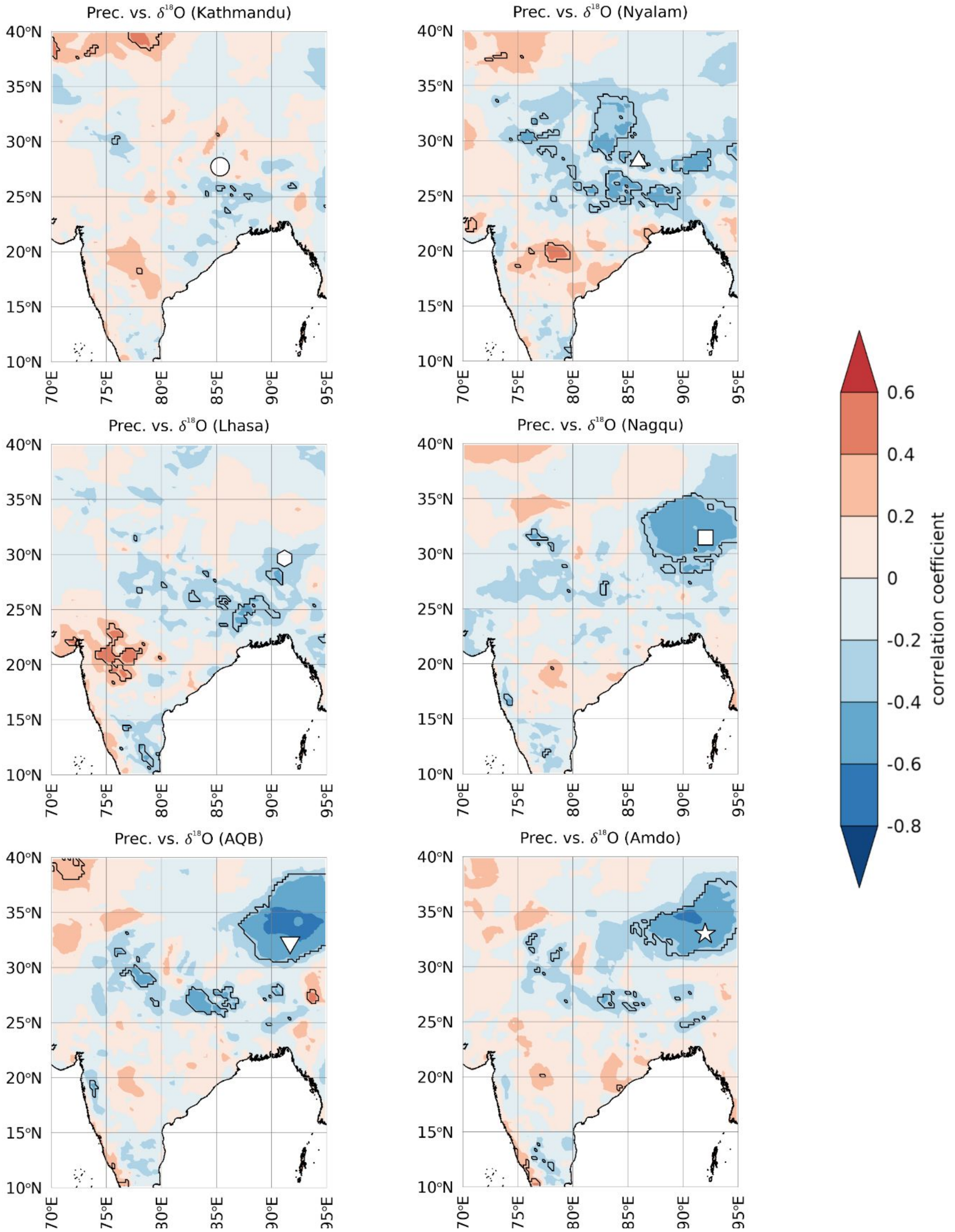

Fig. 6. Correlation coefficients between δ^{18}O in precipitation at each site and precipitation amount. Black contoured regions indicate $p < 0.05$ based on Student's *t*-test. Site positions are represented by a white circle (Kathmandu), triangle (Nyalam), hexagon (Lhasa), square (Nagqu), inverted triangle (AQB), and star (Amdo).

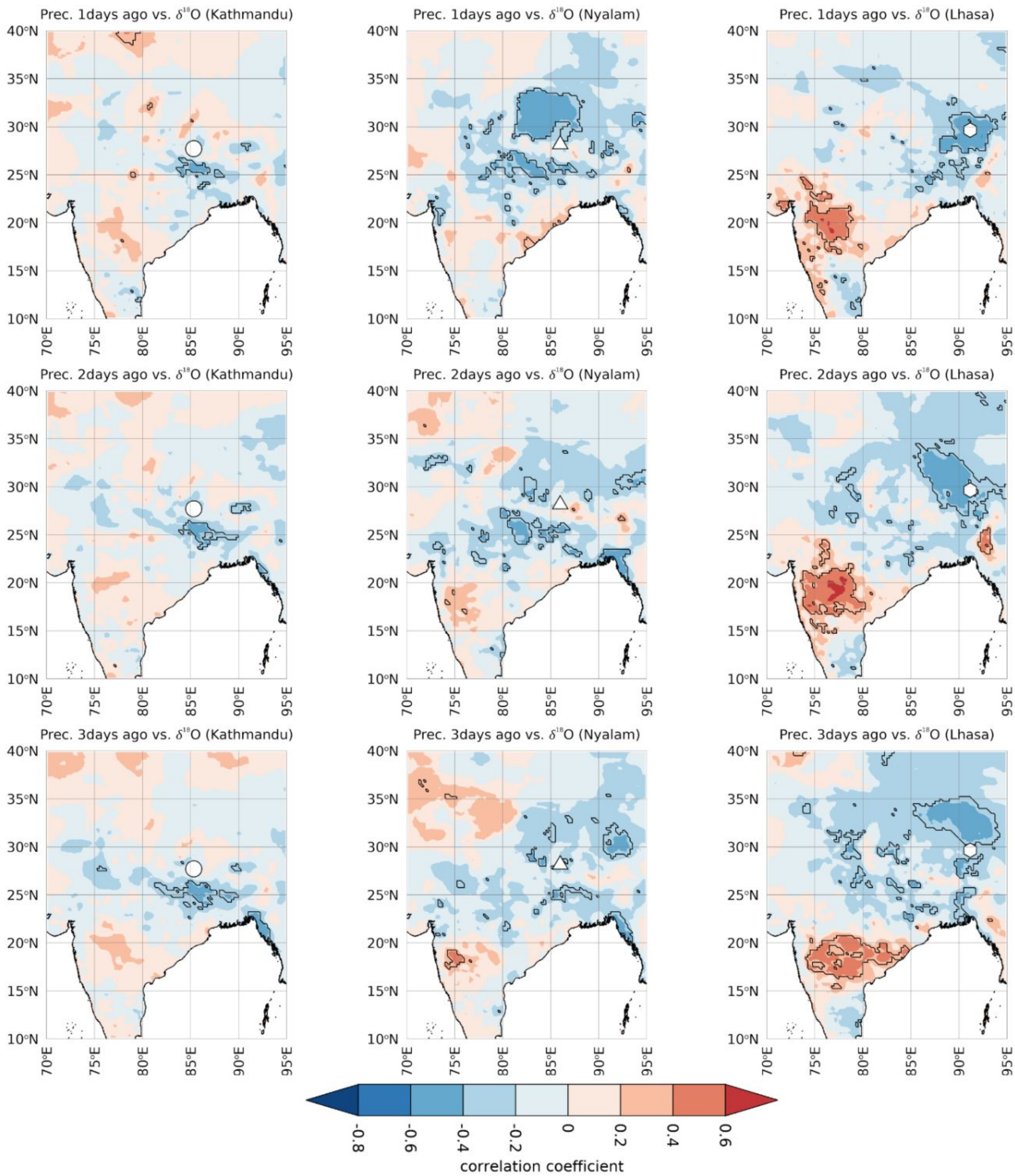

Fig. 7. Correlation coefficients between $\delta^{18}O$ values in precipitation at three sites: Kathmandu (left), Nyalam (center), and Lhasa (right), and precipitation amounts at time lags of one day (top), two days (middle), and three days (bottom). Black contoured regions indicate $p < 0.05$ based on Student's *t*-test. The positions of the sites are represented as follows: white circle (Kathmandu), triangle (Nyalam), and hexagon (Lhasa).

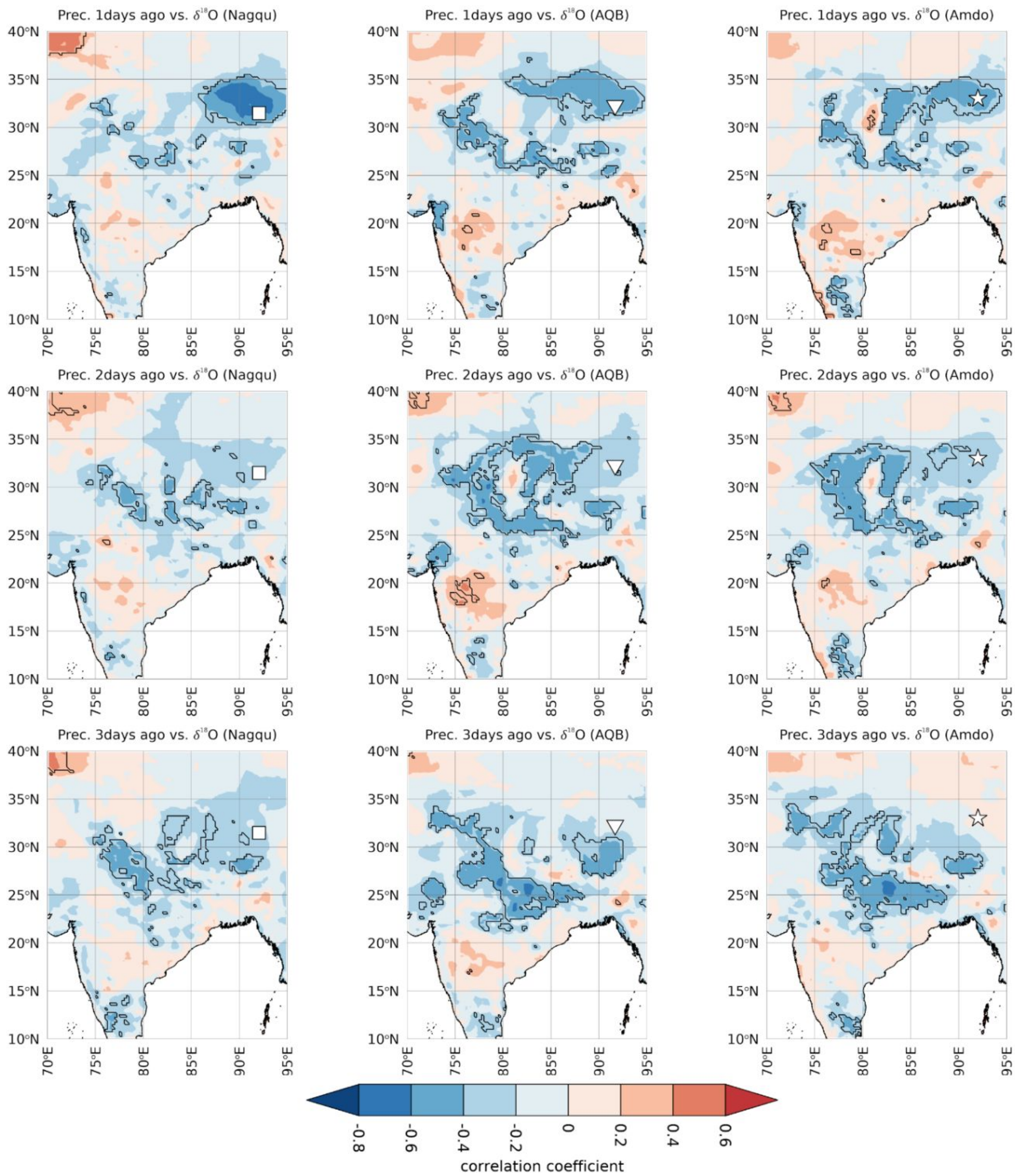

Fig. 8. Correlation coefficients between δ^{18}O values associated with Indian monsoon precipitation at three sites: Nagqu (left), AQB (center), and Amdo (right), and precipitation amounts at time lags of one day (top), two days (middle), and three days (bottom). Black contoured regions indicate $p < 0.05$ based on Student's t-test. Site positions are indicated by a white square (Nagqu), inverted triangle (AQB), and star (Amdo).

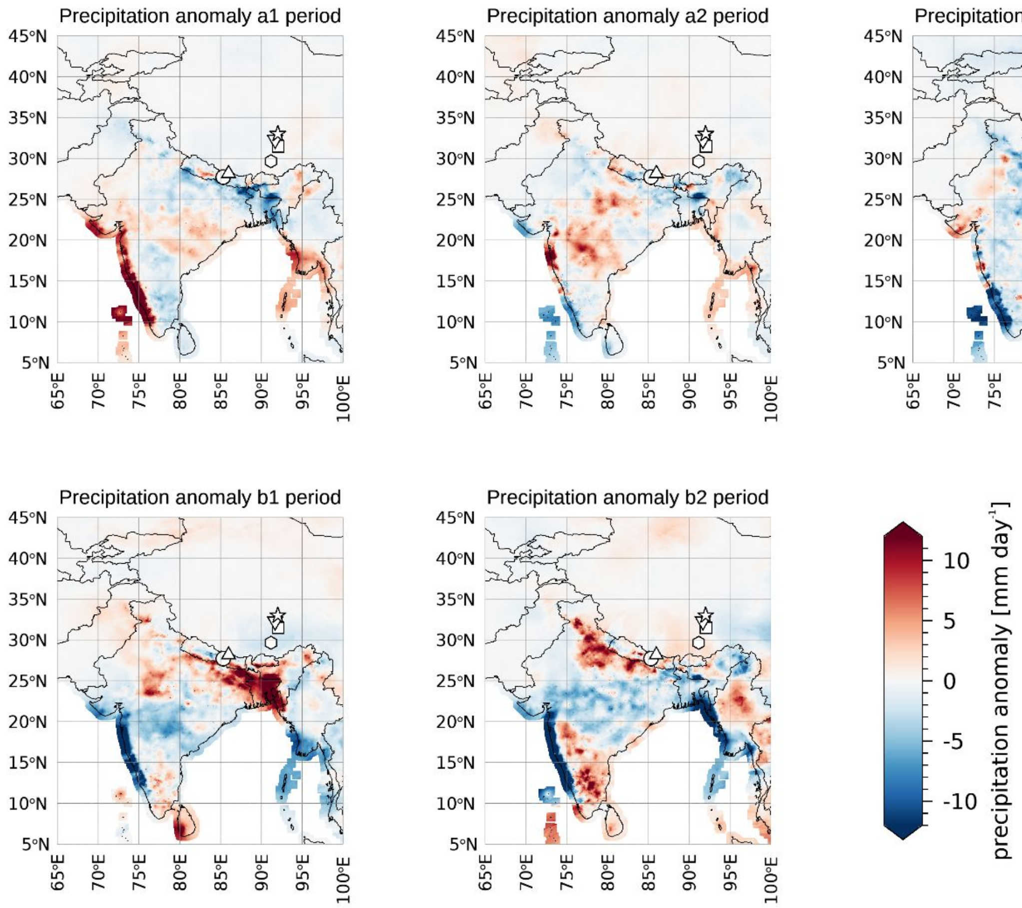

Fig. 9. Mean precipitation anomalies during the active (a1, a2, and a3) and break (b1 and b2) phases of the Indian monsoon, based on the APHRODITE dataset. Daily precipitation anomalies were calculated as the difference between daily precipitation and the mean precipitation over the entire observation period. Site positions are indicated by a white circle (Kathmandu), triangle (Nyalam), hexagon (Lhasa), square (Nagqu), inverted triangle (AQB), and star (Amdo).